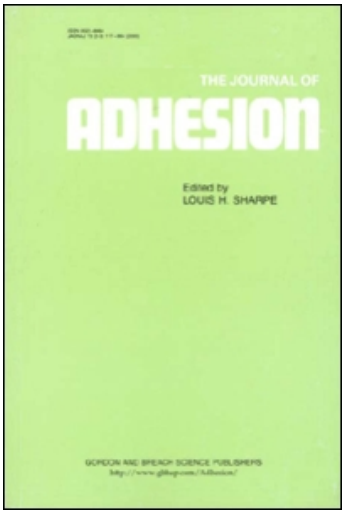

The Journal of Adhesion
Publication details, including instructions for authors and subscription information:
http://www.informaworld.com/smpp/title~content=t713453635

PROBING HIDDEN POLYMERIC INTERFACES USINGIR-VISIBLE SUM-FREQUENCY GENERATION SPECTROSCOPY

Hasnain Rangwalla[a]; Ali Dhinojwala[a]
[a] Department of Polymer Science, Akron, Ohio, USA

Online publication date: 10 August 2010

To cite this Article Rangwalla, Hasnain and Dhinojwala, Ali(2004) 'PROBING HIDDEN POLYMERIC INTERFACES USINGIR-VISIBLE SUM-FREQUENCY GENERATION SPECTROSCOPY', The Journal of Adhesion, 80: 1, 37 — 59
To link to this Article: DOI: 10.1080/00218460490276768
URL: http://dx.doi.org/10.1080/00218460490276768

The Journal of Adhesion, 80: 37–59, 2004

ISSN: 0021-8464 print/1545-5823 online
DOI: 10.1080/00218460490276768

Taylor & Francis
Taylor & Francis Group

PROBING HIDDEN POLYMERIC INTERFACES USING IR–VISIBLE SUM-FREQUENCY GENERATION SPECTROSCOPY

Hasnain Rangwalla
Ali Dhinojwala
Department of Polymer Science, University of Akron,
Akron, Ohio, USA

Understanding the molecular-level processes underlying interfacial phenomena is important in the area of adhesion. We briefly introduce IR–visible sum-frequency generation spectroscopy (SFG) using a total-internal-reflection geometry for the study of polymer–air, polymer–solid, and polymer–polymer interfaces. The following examples, predominantly of work done in our lab, illustrating differences in molecular structure and dynamic properties at interfaces are presented: the air- and solid-interface structure of an amorphous polystyrene (PS) and a semicrystalline polymer with side-chain crystallinity, poly(octadecyl acrylate) (PA-18); structure of a polymer–polymer interface between thin films of a semicrystalline polymer with side-chain crystallinity, poly(vinyl-N-octadecylcarbamate-co-vinyl acetate), and an amorphous PS; thermal order-to-disorder transitions of the air and solid interface of PA-18, and the interface of this polymer with PS; and dynamic surface-relaxation studies of a rubbed PS film.

Keywords: Polymer adhesion; Polymer surface; Polymer interface; Alkyl side chain polymer; Surface restructuring; Surface transition; Nonlinear optics; Sum frequency generationfs

Received 22 August 2003; in final form 6 November 2003.

We gratefully acknowledge funding from NSF-DMR 9984996, 3M Corporation, and Petroleum Research Funds. We thank Dr. Mesfin Tsige (Sandia National Laboratories) for many helpful discussions of their PDMS simulation results.

One of a collection of papers honoring Jacob Israelachvili, the recipient in February 2003 of *The Adhesion Society Award for Excellence in Adhesion Science, Sponsored by 3M*.

Address correspondence to Ali Dhinojwala, Department of Polymer Science (3909), University of Akron, Akron, OH 44325-3909, USA. E-mail: ali4@uakron.edu

INTRODUCTION

Often in scientific or technological areas governed by physicochemical principles—areas such as adhesion, coatings, catalysis, cell biology, and biomedical implants—there are problems that involve the coming together of two immiscible substances [1–3]. The boundary region at which the phases of such substances meet is defined as the *interface*[1] [4]. Observable interfacial phenomena are dictated by the nature and organization of molecules originating from each of the two phases and residing in the interface. In most instances, the latter is inferred from the former—for example, wettability studies and friction measurement may suggest the preference of certain types of molecules, and perhaps even their structure, at the interface [2]. Knowledge of the underlying molecular origins is important because the composition and architecture of molecules can be controlled by chemical synthesis; therefore, proven molecular mechanisms for interfacial phenomena are of great value in controlling the behavior of two substances at their mutual interface. However, because several buried or hidden interfaces (*e.g.*, solid–solid and solid–liquid) are inaccessible *in situ* by conventional surface science techniques that require vacuum, traditionally researchers have resorted to indirect and *ex situ* routes [2, 3, 5–7] to obtain the molecular-level picture.

In the last two decades, investigators have taken advantage of second-order, nonlinear optical effects—second-harmonic generation (SHG) and sum-frequency generation (SFG)—as a new route to probe buried interfaces because these effects are very often confined to the interfacial regions of samples (explained below). In this report, we concentrate on some innovative uses of SFG measurements, done in our lab, in example applications that are relevant to the science and technology of adhesion. Recent SFG review articles by Chen *et al.* [8] and Buck and Himmelhaus [9] are noteworthy; they cover a broader range of applications as well as the published work of several research laboratories. With the applications discussed here, we hope to elucidate the utility of SFG in knowing molecular-level structure and processes that can contribute to the understanding of adhesion. Because of the extensive use of polymers in adhesion, all examples selected consist of polymeric interfaces, wherein either one or both of the bulk phases are polymeric. However, before we discuss these examples,

[1]A conventional usage of the word *surface* is to represent the outermost region of a bulk phase that is in direct contact with a gas phase (usually air), and for the word *interface* is to represent the thin region of contact between two condensed phases (such as a solid and a liquid). In this report we use the word interface to represent both.

we present a short background on SHG and SFG and their inherent advantages for interfacial studies.

Nonlinear optical phenomena were first realized in the laboratory after the advent (late 1950s) of pulsed lasers that are able to generate high-intensity electric fields. SHG and SFG are the two commonly encountered nonlinear optical techniques. In SHG (Figure 1a), a laser-light beam at frequency ω is converted to a beam at twice the frequency, 2ω. In SFG (Figure 1b), laser-light beams of frequencies ω_1 and ω_2 are overlapped in a medium to produce a beam at the sum of the two source frequencies, $\omega_3 = \omega_1 + \omega_2$. The light sources do not have to be lasers, but in practice only pulsed lasers can produce the high-intensity electric fields required to generate detectable outputs.

These nonlinear effects were first demonstrated in bulk media—SHG in 1961 [10] and SFG in 1962 [11]. It was only much later that they were applied to study surfaces, 1974 for SHG [12] and 1987 for SFG [13]. When it comes to probing interfaces, SFG is preferred over SHG, because by using a tunable IR laser as one of the light sources (at frequency ω_2) a vibrational spectrum of the molecular species located just at an interface can be obtained. This has resulted in the rapid evolution of a whole new spectroscopy since the first demonstration in 1987 by Zhu *et al.*, and it is commonly known as IR–visible sum-frequency generation spectroscopy (or SFG in the text below).

SFG is based on a second-order nonlinear process; therefore, it is for–bidden in media with inversion symmetry, such as the bulk of gases, liquids, and most solids, assuming the *electric-dipole approximation*, which neglects the signal generated by multipoles and magnetic moments. However, at the interface between two centrosymmetric media, inversion symmetry is necessarily broken and generation of the SFG signal is allowed. This is why the spectra represent a thin layer of molecules at the interface of bulk phases. Because it uses beams of visible and infrared light, SFG is useful in probing buried interfaces *in situ*. The only requirement for SFG is that light at frequencies ω_1

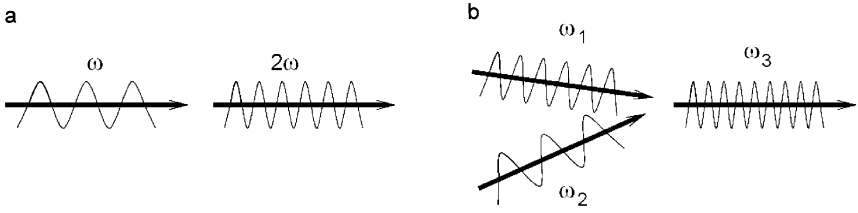

FIGURE 1 Conceptual illustration of the (a) SHG and (b) SFG nonlinear optical effects.

and ω_2 should be able to access the interface, and light at frequency ω_3 should be able to leave the interface through one of the adjoining phases and be measured by a suitable detector. Besides indicating the presence of various chemical species (composition) at interfaces, SFG spectra can also determine the spatial orientation of these species at the interface; therefore, SFG gives useful structural information for interfaces at the molecular level, which can be pivotal in understanding the microscopic origins of macroscopic phenomena such as friction, tack, and wettability. Furthermore, SFG is a nondestructive technique for most potential applications because the laser intensities are not high enough to damage the interface being probed.

These advantages have led to the rise of SFG as the method of choice in many interfacial studies. We next provide a rudimentary introduction to the theory of SFG and some of the commonly used geometries in studying buried interfaces.

THEORY OF SURFACE-SENSITIVE SFG

The theory of SFG has been explained in published works [14–17] and is not presented here at the same level of detail. Although the following background information is succinct, we believe it is sufficient for enabling the uninitiated reader to appreciate the examples and case studies presented in the text.

If the molecules of a medium are subjected to an intense electric field (*e.g.*, Figure 1a), then the region of the medium so exposed will get polarized according to

$$\mathbf{P} = \varepsilon_0(\chi^{(1)} \cdot \mathbf{E} + \chi^{(2)} : \mathbf{EE} + \chi^{(3)} \vdots \mathbf{EEE} + \cdots). \quad (1)$$

Here, $\mathbf{P}$ is the polarization vector, $\mathbf{E}$ is the electric field vector, and $\chi^{(1)}$, $\chi^{(2)}$, and $\chi^{(3)}$ are, respectively, the first-, second-, and third-order electric susceptibility tensors of the medium (higher order susceptibilities are not shown and are usually negligible in magnitude). Note that this expression neglects contributions from multipoles (*e.g.*, quadrupole) and magnetic moments, and this omission is called the *electric-dipole approximation*. Also, it is assumed that the medium does not have a static polarization (true for most materials).

If a region of the medium is simultaneously subjected to two intense electric fields, $\mathbf{E}_1$ and $\mathbf{E}_2$, then the induced polarization, $\mathbf{P}$, contains the term $\chi^{(2)} : (\mathbf{E}_1\mathbf{E}_2 + \mathbf{E}_2\mathbf{E}_1)$. When the source of electric fields is laser light, as in Figure 1b, $\mathbf{E}_1 = \mathbf{E}_1^0 \cos(\omega_1 t)$ and $\mathbf{E}_2 = \mathbf{E}_2^0 \cos(\omega_2 t)$. In this case, it is easily seen with a trivial trigonometric rearrangement that the term containing $\chi^{(2)}$ will have a sinusoidal component of frequency

$\omega_1 + \omega_2$; this component of the polarization will generate electromagnetic radiation at frequency $\omega_1 + \omega_2$, which is the sum-frequency generation signal. Unlike optical processes such as Raleigh and Raman scattering, SHG and SFG generate a coherent signal in the form of a collimated beam in a predictable direction; this is advantageous because it allows for the spatial filtering of incoherent background noise. From symmetry arguments it can be shown that the third-rank tensor, $\chi^{(2)}$, has a value of **0** in centrosymmetric media. Then, under the electric-dipole approximation only $\chi^{(2)}$ contributes to the SFG signal, so in centrosymmetric media the SFG signal is forbidden. This is why SFG is forbidden in the bulk of most substances, which are centrosymmetric, but it is allowed at the interface between bulk phases where there is a breakdown of centrosymmetry.

Figure 2 shows a simple geometry for SFG that is commonly used. Here, the visible and IR beams are moving in the same direction along the x axis (copropagating), and all three beams are in the same plane, the plane of incidence. The ω_1 and ω_2 beams are either S- or P-polarized; S means the electric field of the light beam is perpendicular to the plane of incidence (along the y axis), and P means the field is in the plane of incidence (the xz plane). The signal-beam polarization is also set to S or P by the polarizer (L) before the beam reaches the detector (T). The combination of polarizations of all three beams is given by a sequence of three letters, each being S or P (*e.g.*, SSP), with the letters (first to last) indicating the polarization of the SFG beam, visible beam, and IR beam. The polarization settings in SFG play an important role in selectively probing different components of $\chi^{(2)}$ (discussed below).

If $I(\omega_i)$ is the intensity of a beam at frequency ω_i (see Figure 2), then the SFG signal intensity depends on the probing visible- and IR-beam intensities as follows [17]:

$$I(\omega_3 = \omega_1 + \omega_2) \propto \left|\chi^{(2)}_{\text{eff}}\right|^2 I(\omega_1) I(\omega_2). \tag{2}$$

Here, $\chi^{(2)}_{\text{eff}}$ (or χ_{eff} for simplicity) is an effective, second-order, nonlinear susceptibility of the interface; it is a sum of terms in which each term contains a single component of the second-order susceptibility tensor, $\chi^{(2)}$, of the interface; the components are $\chi_{ijk}(\omega_2)$ (or χ_{ijk} for simplicity), where $i,j,k = x,y,z$ (x, y, and z are the lab axes in Figure 2, and, from here on the indices *ijk* appearing together will have this meaning). For an interface with azimuthal, or $x-y$, isotropy (such as all the interfaces described below) only 7 combinations out of the 27 possibilities of *ijk* in χ_{ijk} are nonvanishing, and only four are independent [17]: $\chi_{xxz} = \chi_{yyz}$, $\chi_{xzx} = \chi_{yzy}$, $\chi_{zxx} = \chi_{zyy}$, and χ_{zzz}.

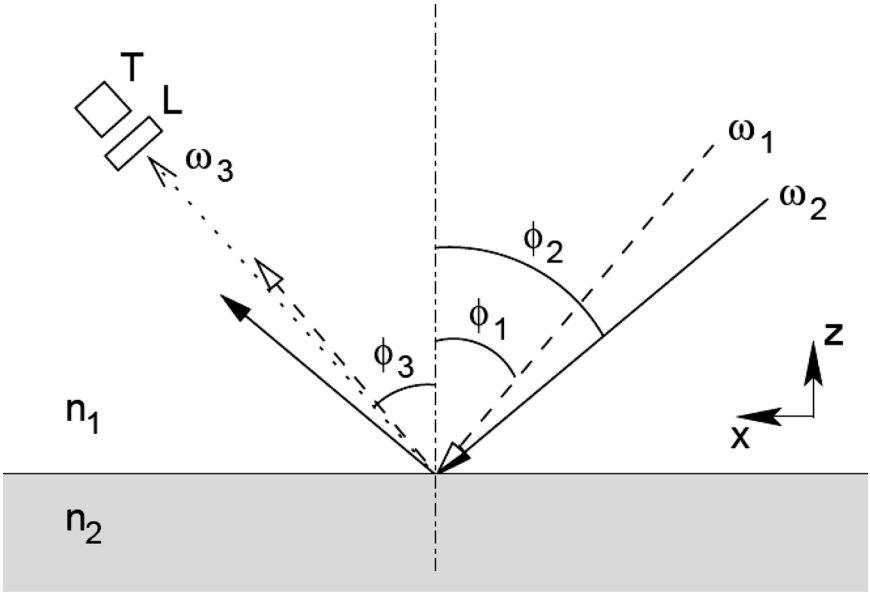

FIGURE 2 Schematic diagram (not to scale) of a copropagating, external-reflection (ER) geometry used for SFG. The beams of frequencies ω_i are as follows: $i = 1$, S- or P-polarized visible; 2, S- or P-polarized IR; and 3, SFG. L is a polarizer and T a photomultiplier detector. The two mediums of refractive indices n_1 and n_2 are as labeled, and their interface is the solid line. x, y, and z are Cartesian axes of the lab frame-of-reference. The y axis is perpendicular to the plane of the paper.

The combination of χ_{ijk}'s that comprise χ_{eff} depend on the beam polarizations: For example, χ_{eff} in SSP polarization consists of just one term containing a single χ_{ijk}:

$$\chi_{\mathrm{eff,SSP}} \propto \chi_{yyz}(\omega_2). \tag{3}$$

The constant of proportionality in Equation (3) has a weak dependence on ω_2, and this dependence is often neglected. This equation shows that in SSP the χ_{yyz} component of the $\chi^{(2)}$ tensor is probed.

The χ_{ijk}'s are each a sum of one nonresonant term and Q resonant terms, one for each vibrational mode of each interfacial species:

$$\chi_{ijk}(\omega_2) = \chi_{ijk}^{\mathrm{NR}} e^{i\Phi} + \sum_{q=1}^{Q} \frac{A_{ijk,q}}{\omega_2 - \omega_q + i\Gamma_q} \tag{4}$$

where $A_{\mathrm{ijk,q}}$, ω_{q}, and Γ_{q} are the amplitude, frequency, and width, respectively, of the resonance q, and Φ is the relative phase of the nonresonant term with respect to the resonant terms. The SFG spectra are usually normalized for the variation in $\mathrm{I}(\omega_1)$ and $\mathrm{I}(\omega_2)$ (Equation (2)). Often, spectra are then fit to Equation (4), and the $A_{\mathrm{ijk,q}}$'s obtained from the fit are then adjusted by any proportionality constant, such as in Equation (3).

The $A_{\mathrm{ijk,q}}$'s have their origins in the molecular hyperpolarizability-tensor (β) components, which are as follows[2]:

$$\beta_{lmn}(\omega_2) = \sum_{q=1}^{Q} \frac{\beta_{lmn,q}}{\omega_2 - \omega_q + \mathrm{i}\Gamma_q} \tag{5}$$

where $l, m, n = a, b, c$. Here, a, b, and c are axes of the Cartesian frame-of-reference that is fixed to the molecule; c is conventionally taken to coincide with the axis (or one of the axes) of highest symmetry of the molecule. $\beta_{\mathrm{lmn,q}} = \mathrm{A_{lm,q}M_{n,q}}$ [18], where $\mathrm{A_{lm,q}}$ is the lm component of the Raman tensor and $\mathrm{M_{n,q}}$ is the n component of the transition-dipole-moment vector. Therefore, only those vibration modes that are both Raman and IR active contribute to the hyperpolarizability tensor, *i.e.*, only such modes are SFG-active.

The $\beta_{\mathrm{lmn}}(\omega_2)$ (or β_{lmn}'s for simplicity) can be projected on the lab axes (xyz) given the orientation of the abc axes with respect to the xyz axes. This orientation is conveniently expressed using the Euler angles (ψ, θ, ϕ) $= \Omega$ [15]. Knowing Ω, the 27×27 projection coefficients $\mathrm{U_{ijk:lmn}}(\Omega)$ can be determined and applied to obtain per-molecule components of β in the xyz frame as follows:

$$\beta_{ijk}(\omega_2, \Omega) = \sum_{l,m,n=a,b,c} U_{ijk:lmn}(\Omega)\beta_{lmn}(\omega_2). \tag{6}$$

The resonant portion of Equation (4) is then a summation of the ijk component of hyperpolarizability for all interfacial molecules:

[2]In Equation (6), and the subsequent expressions that follow, we have assumed that all the vibrational modes, q, belong to a single type of molecular species or moiety. Although this is usually not true, the extension for the case of multiple types of species is trivial. The more general treatment would unnecessarily increase the complexity of the notation.

$$\sum_{q=1}^{Q} \frac{A_{ijk,q}}{\omega_2 - \omega_q + i\Gamma_q} = \sum_{\text{molecules}} \beta_{ijk}(\omega_2, \Omega) = N\langle \beta_{ijk}(\omega_2, \Omega) \rangle = N \int \beta_{ijk}(\omega_2, \Omega) f(\Omega)\, d\Omega. \quad (7)$$

Here, N is the total number of such molecules, $\langle\rangle$ indicates an ensemble average, and $f(\Omega)$ is the probability distribution function of the molecular orientation. The tilt of the molecular c axis from the surface normal (z axis), θ, is of particular significance because often the molecules at the interface can be assumed to have azimuthal isotropy (randomly distributed in ψ and ϕ); in such cases, Ω in Equation (7) can be replaced by θ (we shall assume this in what follows).

Substituting from Equations (6) and (5) in Equation (7) gives

$$A_{ijk,q} = N \int \left[\sum_{l,m,n=a,b,c} U_{ijk:lmn}(\theta) \beta_{lmn,q} \right] f(\theta)\, d\theta. \quad (8)$$

Usually f(θ) is assumed to be a Gaussian distribution, and clever methods to estimate the above integral have been devised [19]. Equation (8) shows the intimate connection between the components of the macroscopic susceptibility tensor, $\chi^{(2)}$, and its molecular counterpart, the microscopic hyperpolarizability tensor, β, of the molecular species that make up the interface. Herein lies the ability of SFG to determine the orientation of interfacial species. With a knowledge of $A_{\text{ijk,q}}$ (obtained from SFG spectra), $\beta_{\text{lmn,q}}$ (obtained from linear spectroscopies or computational methods), and a solution to Equation (8), it is often possible to determine the tilt of molecular species, θ, at the interface by taking ratios of appropriate $A_{\text{ijk,q}}$'s, and eliminating N; in some cases, the ratio of $A_{\text{ijk,q}}$'s is independent of $\beta_{\text{lmn,q}}$'s, and it is possible to obtain θ without knowing any $\beta_{\text{lmn,q}}$.

Figure 3 shows another commonly used geometry for SFG measurements, called the total internal reflection (TIR) geometry; the figure shows an example of a polymer–polymer interface being probed by SFG. Here, one face of an equilateral, sapphire prism has two films of different polymers coated on it. The prism is then mounted on a cell (not shown) of an appropriate construction, and the incoming laser beams (at ω_1 and ω_2) are aligned as shown. The angles $\phi_{\text{A,1}}$ and $\phi_{\text{A,2}}$ are selected so that the incident and reflected angles at the polymer 1–polymer 2 (C) interface—$\phi_{\text{C,1}}$, $\phi_{\text{C,2}}$, $\phi_{\text{C,3}}$—are close to the critical angles for the visible, IR, and SFG frequencies at this interface. This set of ϕ_{C}'s greatly enhances the SFG signal from the C interface while

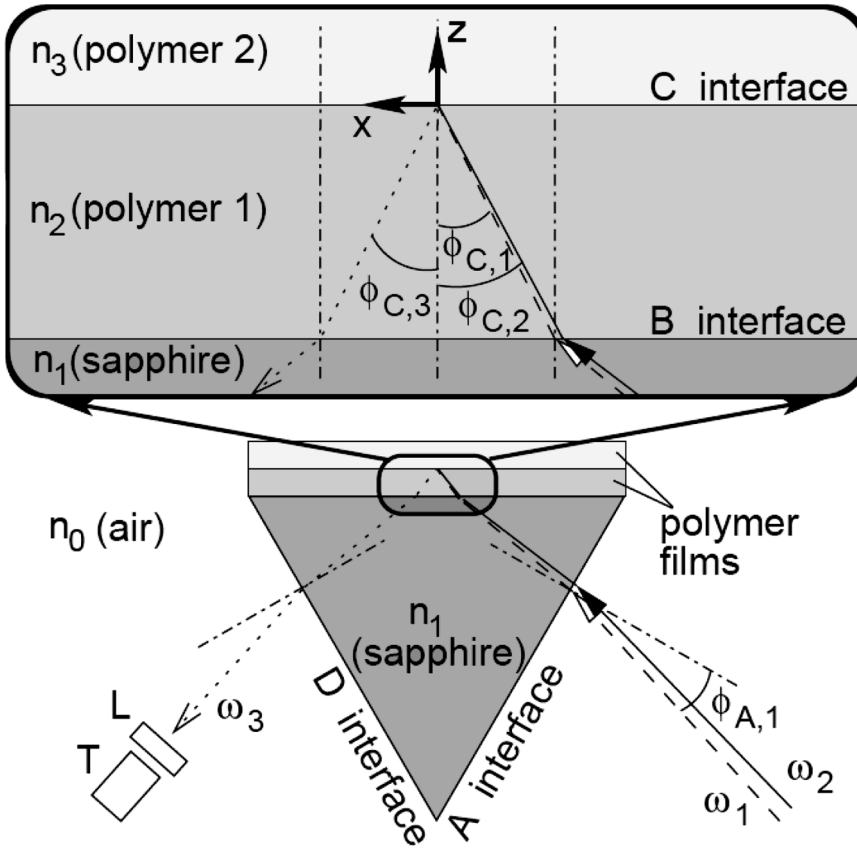

FIGURE 3 Schematic diagram (not to scale) of a TIR geometry used for SFG of a polymer–polymer interface. The beams of frequencies ω_i, the elements L and T, and the *xyz* axes have the same meaning as in Figure 2. The mediums of refractive indices n_i are as labeled. The interfaces formed at the boundaries of these mediums are as follows: A and D, sapphire–air; B, polymer 1–sapphire; C, polymer 1–polymer 2. The incident angles (ω_1 and ω_2 beams) and the reflected/refracted angles (ω_3 beam) at these interfaces are denoted by $\phi_{\text{interface,i}}$.

reducing any interfering signal from the polymer 1–sapphire (B) or polymer 2–air (D) interfaces [20, 21]. Therefore, proper choice of ϕ_A's allows the selective probing of the C interface, but by choosing other values of ϕ_A's it is possible to selectively probe the B and the D interfaces, too. The setup shown here is for a polymer–polymer interface, but by replacing polymer 2 by a liquid (*e.g.*, water) or gas (*e.g.*, air),

the polymer–liquid and polymer–gas interfaces can also be probed by appropriate selection of ϕ_A's. Hence, we can appreciate the versatility of the TIR geometry.

SELECTED EXAMPLES

Differences in Molecular Structure at Polymer–Air and Polymer–Sapphire Interfaces

Gautam *et al.* [22] were the first authors to apply SFG as a probe of a hidden polymer–solid interface. They studied the interfaces formed by a thin polystyrene (PS) film on one face of a sapphire prism. Figure 4 demonstrates the application of SFG in TIR geometry (the schematic of their geometry can be obtained simply from Figure 3 by replacing the polymer 2 medium with air) to probe the PS–air and PS–solid interfaces. The two wavenumbers of 3027 and 3067 cm^{-1} were chosen because the strongest SFG signals for the PS–sapphire and PS–air interfaces, respectively, were observed at these wavenumbers (Figure 5). It is clear that the SFG intensity is enhanced near the angles 7° (PS–sapphire) and 44° (PS–air); these values of $\phi_{A,1}$ (with $\phi_{A,2} \approx \phi_{A,1} - 1.5^\circ$) result in incidence angles of the visible and IR beams to be near their respective critical angles at the PS–sapphire interface (B interface in Figure 3) when $\phi_{A,1} = -6^\circ$ and at the PS–air interface (C interface) when $\phi_{A,1} = 44^\circ$.

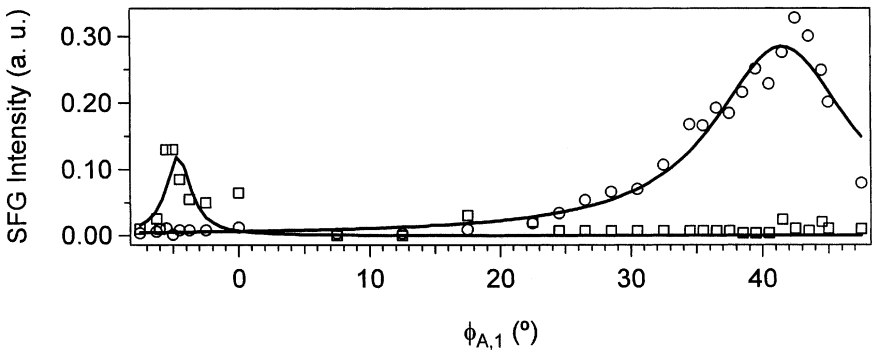

FIGURE 4 The SFG intensity in SSP polarization of a thin, PS film on one face of a sapphire prism (TIR geometry). The intensity is plotted as a function of incident angle $\phi_{A,1}$ (Figure 3, where $\phi_{A,2} \approx \phi_{A,1} - 1.5^\circ$) for two values of the IR wavenumber, ω_2: 3027 cm^{-1} (squares) and 3067 cm^{-1} (circles). The circle data are scaled up by a factor of five. The solid lines are a guide to the eye. (Adapted from Gautam *et al.* [22].)

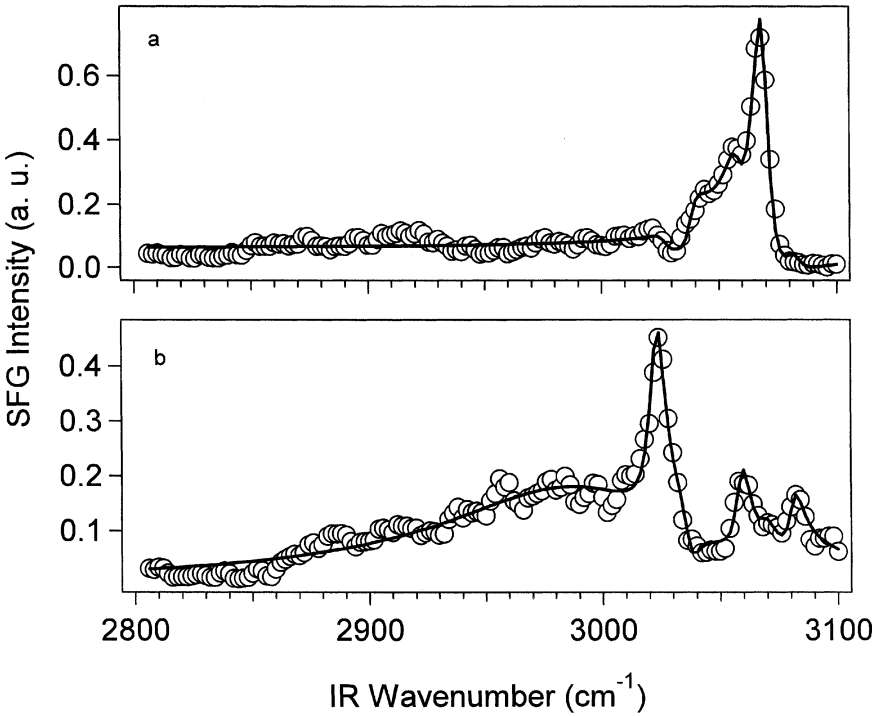

FIGURE 5 SFG spectra in SSP polarization for the (a) PS–air interface ($\phi_{A,1}$ in Figure 3 was 44°) and (b) PS–sapphire interface ($\phi_{A,1} = -6°$); $\phi_{A,2} \approx \phi_{A,1} - 1.5°$ in both cases. The solid lines are fits of the data to Equation (4). (Adapted from Gautam *et al.* [22].)

To obtain the intensities of the SFG-active vibrational resonances of both the interfaces, SFG spectra of the PS–air and PS–sapphire interfaces were obtained (Figure 5) as a function of IR frequency, ω_2, by fixing the incidence angles to the optimum values mentioned above. A sharp resonance at 3069 cm^{-1}, assigned to the v_2 vibrational mode, dominates the air-interface spectrum of PS. In comparison, the sapphire-interface spectrum shows a strong resonance at 3023 cm^{-1}, assigned to the v_{20b} mode. Noteworthy is the absence of methylene peaks in both spectra: these peaks, at 2850 cm^{-1} and 2920 cm^{-1}, are strong in the IR spectrum of PS. To confirm that this technique is measuring two separate interfaces, the SFG spectra before and after a short plasma treatment were obtained (Figure 6). As expected, the buried PS–sapphire interface is not influenced by the plasma treatment; in contrast, the PS–air interface spectrum after the plasma

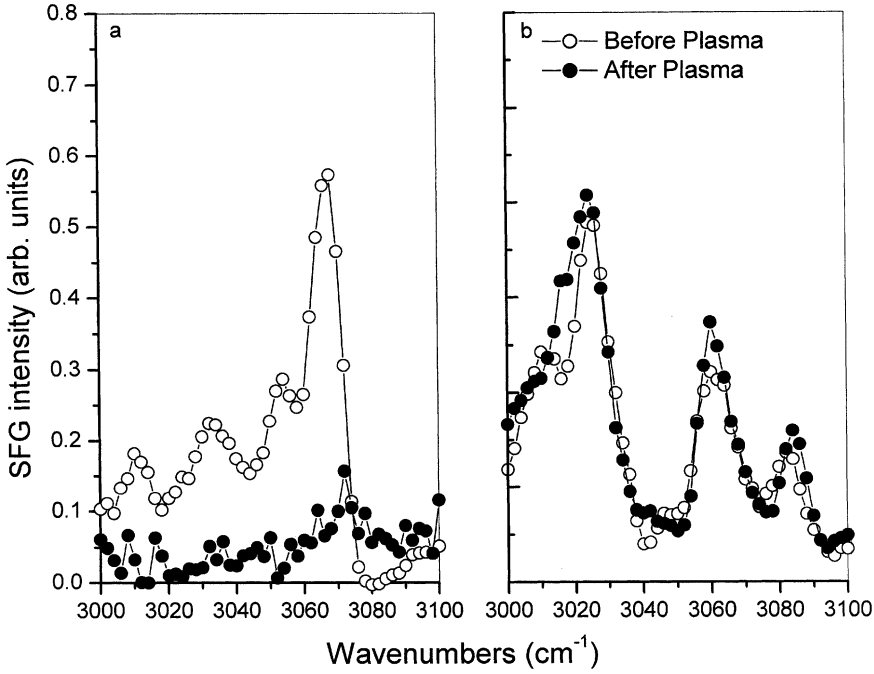

FIGURE 6 SFG spectra (PPP polarization) of the (a) PS–air and (b) PS–sapphire interfaces before (open circles) and after (filled circles) exposure to an argon plasma. The solid lines are guides to the eye. (Gautam, K. S., Schwab, A. D., Dhinojwala, A., Zhang, D., Dougal, S. M., and Yeganeh, M. S., *Phys. Rev. Lett.*, **85**, 3854–3857 (2000). Copyright (2000) by the American Physical Society.)

treatment shows that the initial molecular structure is lost, as expected, for this interface; this confirms the ability of TIR geometry to selectively probe hidden interfaces.

The ratio of $\chi_{yyz,v2}/\chi_{yyz,v20b}$ obtained from the fits can be used to determine the tilt angle of phenyl groups at the air or sapphire interface. Since the v_2 peak is far stronger at the air interface in comparison with the sapphire interface, the phenyl groups are oriented more vertical than at the sapphire interface. In contrast, the absence of the methylene peaks indicates weak orientation of the methylene groups near the surface. Simulation results [23] on free-standing, amorphous, atactic PS films are consistent with the experimental observations that the phenyl rings near the surface point outwards, as shown in Figure 7. The order parameter used is $\langle\cos\theta\rangle$. For the phenyl group (Figure 7a), θ is the angle between the surface normal (z axis) and a

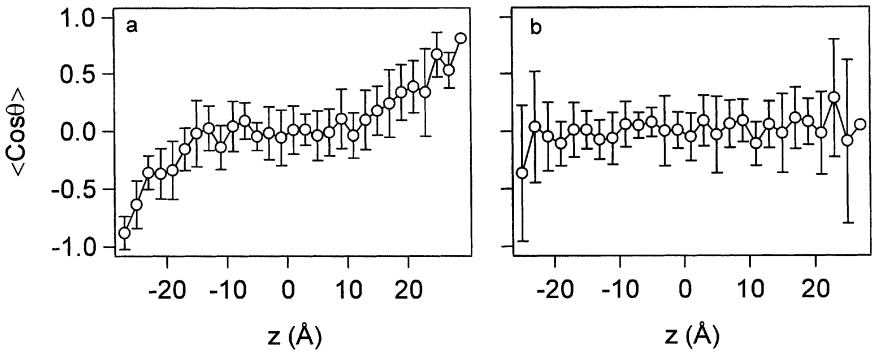

FIGURE 7 Orientational order parameter, obtained by Monte Carlo simulation, as a function of position along the thickness of a thin, free-standing, polystyrene film: (a) The C_2 symmetry axis of the phenyl group and (b) the C_2 symmetry axis of the methylene groups. The midpoint of the film is at z = 0 Å. (Adapted from Clancy *et al.* [23].)

vector in the ring that points from the carbon atom bonded to the polymer backbone to the carbon atom in the para position; for the methylene group (Figure 7b), θ is the angle between the z axis and the group bisector. The order parameter, $\langle\cos\theta\rangle$, is 1 if these vectors point in the positive z direction, -1 if they point in the negative z direction, and 0 for no preferred orientation. For the phenyl groups, the order parameter is close to 1 (-1) near the top (bottom) surface and quickly drops to 0 within a distance of 1–2 nm from the surface. This result confirms the presence of oriented phenyl groups at the PS surface, and also that this order quickly disappears in the bulk. In comparison, the methylene order parameter is approximately equal to zero at the surface and in the bulk, which is consistent with our observation of negligible methylene peaks in the SFG spectra. These results do not imply the presence of well-packed phenyl rings oriented normal to the surface. Instead, one should visualize the results as an ensemble average of phenyl groups oriented anisotropically in the outermost, 1–2 nm thick surface layer. The structure at the PS–air and PS–sapphire interfaces in the glassy state are very similar to that above the glass transition temperature, T_g, of PS [22]. The orientation of phenyl groups at the interfaces is an inherent property of even liquid-like polymer films and is not a consequence of cooling the surface down below its T_g.

Now we move on to another example, the air- and sapphire-interface study of a class of semicrystalline polymers, poly(n-alkyl acrylate)s. These polymers exhibit side-chain crystallinity when the alkyl side-chain contains ten or more carbon atoms. Typical uses for such

polymers are in the formation of release coatings in adhesion applications, because the surfaces are hydrophobic and provide good nonstick properties in contact with hydrophilic adhesives. Figure 8 shows the SFG spectra of the poly(octadecyl acrylate) (PA-18)–air and PA-18–sapphire interfaces, respectively; these spectra were acquired in a TIR geometry in a manner similar to that described for the PS example above. Figure 8a shows two prominent peaks assigned to the methyl vibrations at 2875 cm^{-1} (methyl symmetric) and 2935 cm^{-1} (methyl Fermi-resonance, called methyl Fermi in the text). The absence of methylene vibrations in the spectrum indicates that the alkyl side chains are in predominantly all-trans conformations, similar to those observed for self-assembled monolayers [24, 25]. The ratio of χ_{yyz} for the asymmetric to symmetric methyl vibrations indicates that the –C–C–C– axis is oriented normal to the surface. The crystalline packing of alkyl side-chains at the surface is confirmed by grazing incidence X-ray diffraction measurements using a synchrotron X-ray source, which shows a strong diffraction peak with a d-spacing of 4.2 Å [26]. This crystalline packing

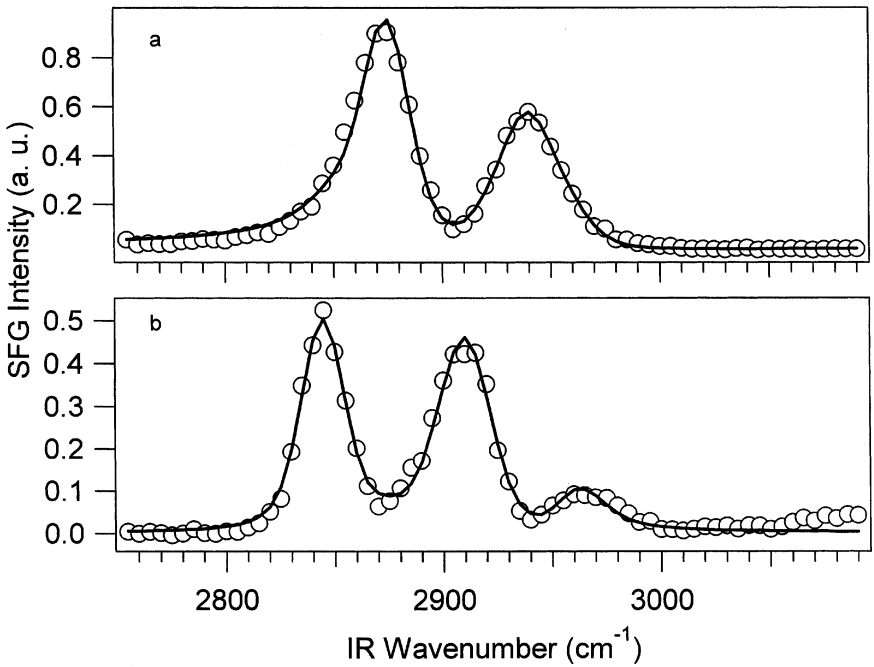

FIGURE 8 SFG spectra (SSP polarization) in a TIR geometry for the (a) PA-18–air interface and (b) PA-18–sapphire interface. The solid lines are fits of the data to Equation (4). (Adapted from Gautam and Dhinojwala [28].)

forms a hydrophobic array of methyl groups at the surface, which is confirmed by high water contact angles of $\approx 110^\circ$ [27].

In comparison, the SFG spectrum for the PA-18–sapphire interface in Figure 8b shows predominantly methylene bands: methylene symmetric, methyl Fermi, and asymmetric bands at 2845, 2895, and 2915 cm^{-1}, respectively. The presence of asymmetric methylene peaks in the SSP spectrum indicates that the C_2 axes of the methylene groups are tilted with respect to the surface normal. It is surprising that we find strong methylene signals at the PA-18–sapphire interface because an all-trans chain is not expected to show strong methylene signals. Furthermore, the SFG signals are much higher than expected from gauche defects present at the interface. One possible explanation is the extension of orientation of methylene groups over several layers next to the solid interface. This has also been observed in simulation results for a thin film of polydimethylsiloxane (PDMS) in contact with solid surfaces as shown in Figure 9. In the case of PDMS, the order parameter ($\langle \cos\theta \rangle$) next to the solid surface oscillates between positive and negative values, and gradually the amplitude of these oscillations decay to zero. Because of the damping of these oscillations, the net orientational order parameter from all the layers is not zero, and this implies a net orientation of methyl groups with respect to the surface normal. Perhaps this anisotropic orientation is general and even applies, near the solid surface, to the methylene groups in the alkyl side-chains or those in the polymer backbone.

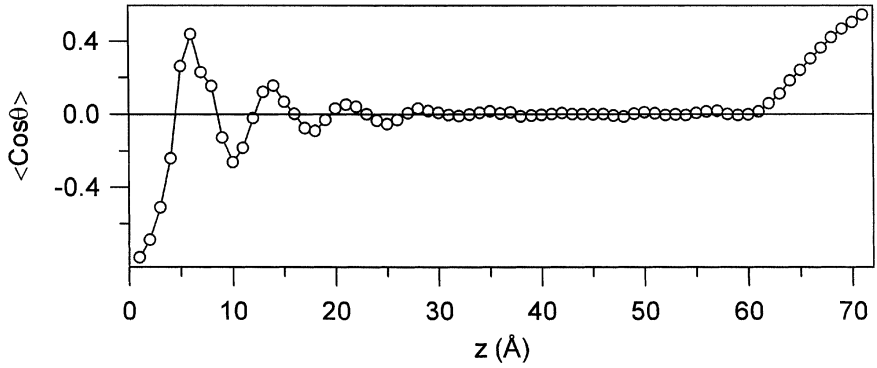

FIGURE 9 Orientational order parameter, obtained by molecular dynamics simulation, as a function of position along the thickness of a thin, PDMS film on a hydroxylated-SiO_2 substrate. The average orientation is for the CH_3 groups (C_3 axis) on the PDMS chains, and $z = 0$ Å is at the boundary of the two phases. (Adapted from Tsige *et al.* [29].)

Probing Polymer–Polymer Interfaces

Harp and coworkers [20, 30] applied SFG to probe a hidden polymer–polymer interface. They studied the interface formed between a thin film of poly(vinyl-N-octadecylcarbamate-co-vinyl acetate) (PVNODC) and a thin film of PS. They used two types of PS in separate measurements: deuterated PS (dPS) and hydrogenated PS (hPS, which is the same as PS in the preceding discussion). Figure 10 shows the SFG spectra acquired in TIR geometry (Figure 3) for these interfaces. To exclude the possibility of SFG-intensity contributions from the PVNODC–air interface in these spectra obtained at an incidence angle of 8°, SFG spectra were also measured at 8° before and after a brief argon plasma treatment; no change was detected in the after-plasma spectrum from the polymer–polymer interface. On the other hand,

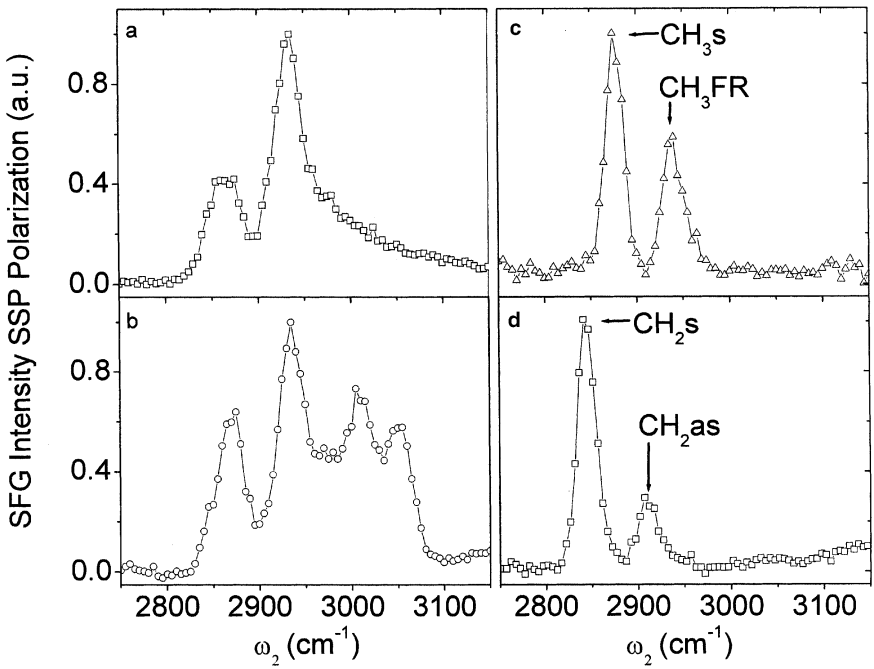

FIGURE 10 SFG spectra in SSP polarization for the (a) PVNODC–dPS interface, $\phi_{A,2}$ (in Figure 3) = 8°; (b) PVNODC–hPS, $\phi_{A,2} = 8°$; (c) PVNODC–air, $\phi_{A,2} = 42°$; and (d) PVNODC–sapphire, $\phi_{A,2} = 8°$. (In all cases, $\phi_{A,1} \approx \phi_{A,2} - 1.5°$.) (c) and (d) were acquired for a solitary film of PVNODC on the sapphire prism. The solid lines are guides to the eye. (Reprinted with permission from Harp, G. P., Gautam, K. S., and Dhinojwala, A., *J. Am. Chem. Soc.* **124**, 7908–7909 (2002). Copyright (2002) American Chemical Society.)

the SFG signals from the PVNODC–air interface of the same samples are reduced 20 to 30 times after plasma treatment. The broad peak at $2865\,cm^{-1}$ corresponds to contribution from methylene symmetric vibration at $2845\,cm^{-1}$ and methyl symmetric vibrations at $2875\,cm^{-1}$. The broad peak at $2935\,cm^{-1}$ corresponds to contribution from methylene asymmetric vibration at $2920\,cm^{-1}$ and methyl Fermi vibrations at $2935\,cm^{-1}$. The presence of methylene peaks is also confirmed using a high-resolution laser system where the methylene and methyl peaks are detected separately [30]. In the case of PVNODC–hPS, two additional peaks are observed above $3000\,cm^{-1}$, corresponding to phenyl vibrations associated with PS.

The orientations of both the PVNODC and PS side chains are different from those at the PVNODC–air (or PS–air) and PVNODC–sapphire (or PS–sapphire) interfaces, as shown in Figures 10c and 10d (or Figure 5). The prominent bands in the PVNODC–sapphire (Figure 10d) interface spectrum are the methylene symmetric and asymmetric band at 2845 and $2915\,cm^{-1}$. In contrast, the dominant peaks at the PVNODC–air (Figure 10c) interface are the symmetric methyl stretching and methyl Fermi resonance peaks at 2875 and $2935\,cm^{-1}$, respectively. For the PS–air interface, one observes a prominent v_2 peak at $3067\,cm^{-1}$ and at the PS–sapphire interface a strong v_{20b} peak at $3023\,cm^{-1}$. The presence of methylene peaks at PVNODC–hPS (or dPS) spectra and a sharp drop in SFG intensity at the melting point (discussed below) can be explained by the presence of heterogeneities in the PVNODC phase, either parallel or perpendicular to the interface. Heterogeneities parallel to the interface would imply crystalline domains consisting of all-trans alkyl side chains surrounded by grain boundaries with disordered alkyl side chains; heterogeneity perpendicular to the interface would imply disordered alkyl chains at the interface with a crystalline layer underneath.

Measurements of Melting Transitions at Polymer–Air, Polymer–Solid, and Polymer–Polymer Interfaces

The ability to probe hidden interfaces using SFG can also be used to study dynamics of molecules at interfaces. Figure 11 shows the SFG intensity as a function of temperature for three different interfaces of PA-18, where the bulk melting point (T_m) was determined by using differential scanning calorimetry (DSC)[3]. In each case, a specific peak

[3]PA-18*, in Figure 11, is chemically the same as PA-18 and has the same air- and sapphire-interface structure as the latter, but PA-18* has a polydispersity of 3.5 and a T_m of 42.5°C, in comparison with 1.1 and 48.3°C for PA-18.

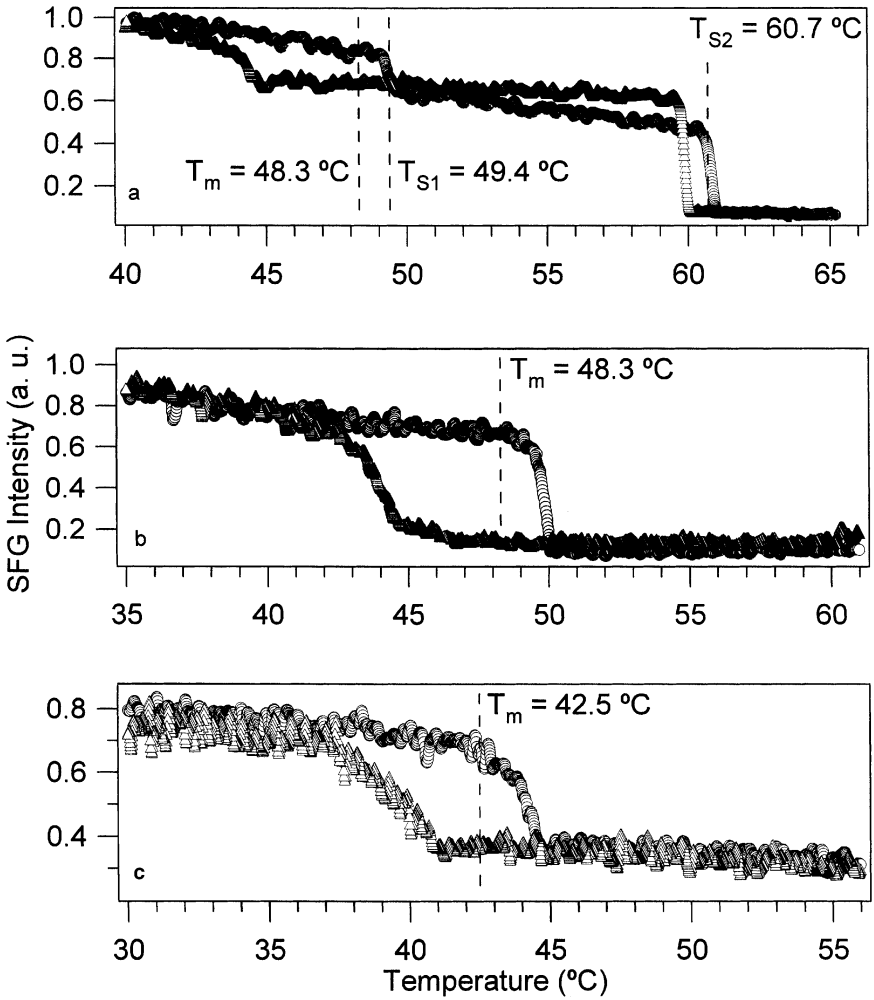

FIGURE 11 SFG intensity as a function of temperature, at fixed IR wavenumbers (ω_2), for the following interfaces: (a) PA-18–air, PPP polarization, $\omega_2 = 2960\,\mathrm{cm}^{-1}$ (methyl asymmetric stretch); (b) PA-18–sapphire, SSP polarization, $\omega_2 = 2845\,\mathrm{cm}^{-1}$ (methylene symmetric stretch); and (c) PA-18*–PS, SSP polarization, $\omega_2 = 2930\,\mathrm{cm}^{-1}$ (methyl Fermi). The interfaces were heated (open circles) and cooled (open triangles) at a rate of 0.3°C/min ((a) and (b)) and 0.5°C/min (c). The dotted, vertical lines mark transition temperatures, which are labeled according to the symbol assigned in the text. ((a) and (b) adapted from Gautam *et al.* [28] and (c) from Harp *et al.* [30].)

assigned to some vibrational mode of the methyl group was chosen in some polarization (SSP or PPP); higher intensities for all peaks represent more order in the methyl groups at the interface, whereas near-zero intensities represent a disordered state of methyl groups and, consequently, the side chains of the PA-18 (PA-18*) polymer. The order-to-disorder transition at the PA-18–air interface is strikingly different from that at the PA-18–sapphire or the PA-18*–PS interface. For the PA-18–sapphire and PA-18*–PS interface, one sharp transition close to the bulk T_m is observed. In contrast, two sharp transitions at the PA-18–air interface are observed. The first transition, T_{S1}, is close to the bulk T_m, and the second, T_{S2}, is 10–20°C (depending on the length of the alkyl side chain) higher than T_m. The shorter the length of the alkyl side chain, the larger the difference between the second transition temperature and the bulk T_m. Furthermore, note that in all cases the reverse transitions during the cooling half-cycle occur at lower temperatures than the corresponding temperature for the heating half-cycle, showing a hysteresis, which indicates some amount of supercooling.

The presence of a unique ordered phase at the PA-18–air interface above T_m has been confirmed using three independent techniques: SFG [28], X-ray reflectivity [26], and grazing-incidence X-ray diffraction (GIXD) [26]. Figure 12 summarizes the findings. Below T_m, both the surface and bulk layer exhibit side-chain crystallinity. The surface alkyl chains are crystalline and ordered. On heating, the bulk melts, leaving a crystalline ordered layer on the surface. At T_{S1}, 1–2°C above bulk T_m, the surface melts into an ordered smectic-like monolayer. On further heating, the smectic-like layer disorders to a liquid state sharply *via* a second transition at T_{S2}, 10–20°C above T_m. This order recovers on cooling with a hysteresis. The presence of an ordered phase above T_m can be explained by the lowering of surface energy due to presence of ordered methyl groups at the surface instead of disordered methyl and methylene groups. Once this driving force is removed, as in the examples of PA-18–sapphire and PA-18*–PS interfaces, the presence of this unique, ordered phase disappears, and, instead, only one transition temperature close to the bulk T_m is observed.

Surface Relaxation of a Rubbed, PS Film

The PS–air spectrum shown in Figure 5 is invariant to rotation in the *xy* plane, and this implies that the orientation of the phenyl groups is isotropic in the *xy* plane. On rubbing the surface with a velour cloth, the phenyl groups reorient so that the planes of the

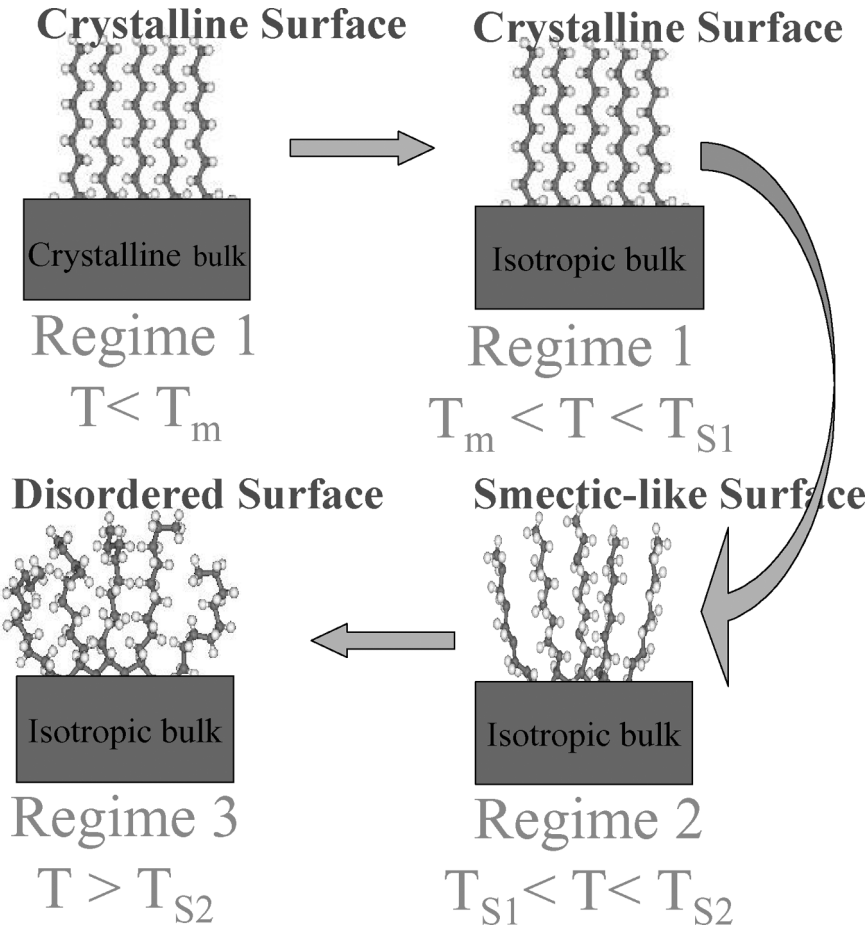

FIGURE 12 Cartoon depiction of the PA-18 surface and the thermal transitions of the surface structure [27].

rings are at ≈90° with respect to the rubbing direction. The resulting SFG intensity is anisotropic with respect to the rotation angle along the *xy* plane. Schwab and Dhinojwala [31] have used the relaxation of these anisotropically orientated phenyl groups to study surface relaxation processes and their relationship with the bulk T_g. Figure 13 shows this relaxation process in the form of a declining SFG-intensity for the ν_2 phenyl vibration mode. On heating, the SFG intensity drops to the value it had before the rubbing process, and on further cooling it remains constant, as expected. The drop-off rate of the SFG signals is modeled using a Kohlrausch–Williams–Watts (KWW)

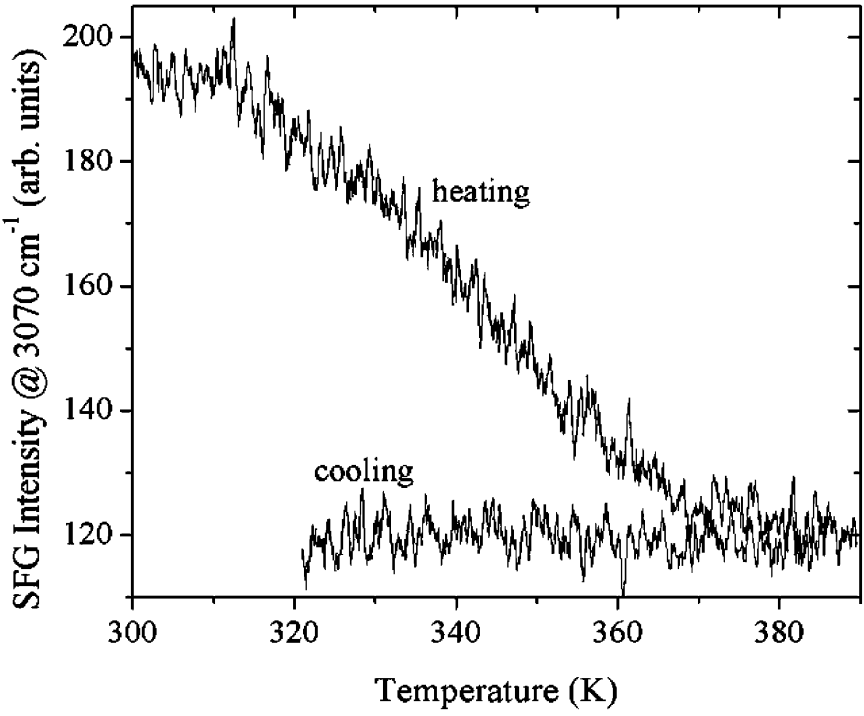

FIGURE 13 Relaxation of the SFG intensity (at 3070 cm^{-1}) from the PS–air interface for a rubbed PS film. The film was heated at the rate of 1°C/min and then cooled at the same rate. (Schwab, A. D. and Dhinojwala, A., *Phys. Rev. E* **67**, 021802/1–10 (2003). Copyright (2003) by the American Physical Society.)

equation and an Arrhenius temperature-dependence below T_g. It was determined that surface groups are much more mobile, have a lower activation energy, and have a larger stretching-exponent than those in the bulk.

SUMMARY

Gaining a molecular-level understanding of interfacial phenomena is important for the ability to control the behavior of two immiscible substances at their mutual interface. This is not only true in the field of adhesion but is a universal requirement for all areas that benefit from surface science. For many cases, such knowledge is hard to acquire *in situ* by conventional experimental methods that require vacuum

because the interface of interest is a buried one. The nonlinear optical technique of SFG has proved to be valuable in several instances that require the direct probing of buried interfaces because the only requirement is that the interface be accessible by visible and infrared light. The salient advantages of SFG are its interface sensitivity, ability to detect molecular species and their orientations, and the ability of probing buried interfaces. SFG in TIR geometry has the added advantages of enhanced signals and the facile selection of different interfaces by choosing appropriate incidence angles for the probing laser-beams.

In this review, with the help of several examples—PS and PA-18 in contact with sapphire and PS in contact with PA-18—we have shown that the molecular structure at the hidden interfaces of polymers are very different from that of the polymer–air or polymer–vacuum interfaces. Conventional techniques that can only analyze the air or vacuum interfaces of these polymers are not capable of revealing these differences. Besides the static structure, the surface relaxation and melting temperatures of the molecules in the interfacial region are also strongly influenced by the nature of the interface.

REFERENCES

[1] Israelachvili, J. N., *Intermolecular & Surface Forces*, 2nd ed., (Academic Press, San Diego, 1991).
[2] Baier, R. E., Shafrin, E. G., and Zisman, W. A., *Science* **162**, 1360–1368 (1968).
[3] Kendall, K., *Science* **263**, 1720–1725 (1994).
[4] Miller, C. A. and Neogi, P. *Interfacial Phenomena: Equilibrium and Dynamic Effects*, volume 17 of Surfactant Science Series, (Marcel Dekker, Inc., New York, 1985).
[5] Wu, S., *Polymer Interfaces and Adhesion* (Marcel Dekker, Inc., New York, 1982).
[6] Maeda, N., Chen, N., Tirrell, M., and Israelachvili, J. N., *Science* **297**, 379–382 (2002).
[7] Morita, M., Ogisu, H., and Kubo, M., *J. Appl. Polym. Sci.* **73**, 1741–1749 (1999).
[8] Chen, Z., Shen, Y. R., and Somorjai, G. A., *Annu. Rev. Phys. Chem.* **53**, 437–465 (2002).
[9] Buck, M. and Himmelhaus, M., *J. Vac. Sci. Technol. A* **19**, 2717–2736 (2001).
[10] Franken, P. A., Hill, A. E., Peters, C. W., and Weinreich, G., *Phys. Rev. Lett.* **7**, 118–120 (1961).
[11] Bass, M., Franken, P. A., Hill, A. E., Peters, C. W., and Weinreich, G., *Phys. Rev. Lett.* **8**, 18–19 (1962).
[12] Simon, H. J., Mitchell, D. E., and Watson, J. G., *Phys. Rev. Lett.* **33**, 1531–1534 (1974).
[13] Zhu, X. D., Suhr, H., and Shen, Y. R., *Phys. Rev. B* **35**, 3047–3050 (1987).
[14] Shen, Y. R., *The Principles of Nonlinear Optics*, (John Wiley & Sons, Inc., New York, 1984), Chapter 6.
[15] Hirose, C., Akamatsu, N., and Domen, K., *Appl. Spectrosc.* **46**, 1051–1072 (1992).
[16] Hirose, C., Akamatsu, N., and Domen, K., *J. Chem. Phys.* **96**, 997–1004 (1992).

[17] Zhuang, X., Miranda, P. B., Kim, D., and Shen, Y. R., *Phys. Rev. B: Condens. Matter* **59**, 12632–12640 (1999).
[18] Watanabe, N., Yamamoto, H., Wada, A., Domen, K., and Hirose, C., *Spectrochim. Acta* **50A**, 1529–1537 (1994).
[19] Simpson, G. J. and Rowlen, K. L., *J. Am. Chem. Soc.* **121**, 2635–2636 (1999).
[20] Harp, G. P., Gautam, K. S., and Dhinojwala, A., *J. Am. Chem. Soc.* **124**, 7908–7909 (2002).
[21] Löbau, J. and Wolfrum, K., *J. Opt. Soc. Am. B* **14**, 2505–2512 (1997).
[22] Gautam, K. S., Schwab, A. D., Dhinojwala, A., Zhang, D., Dougal, S. M., and Yeganeh, M. S., *Phys. Rev. Lett.* **85**, 3854–3857 (2000).
[23] Clancy, T. C., Jang, J. H., Dhinojwala, A., and Mattice, W. L., *J. Phys. Chem. B* **105**, 11493–11497 (2001).
[24] Guyot-Sionnest, P., Hunt, J. H., and Shen, Y. R., *Phys. Rev. Lett.* **59**, 1597–1600 (1987).
[25] Guyot-Sionnest, P., Superfine, R., Hunt, J. H., and Shen, Y. R., *Chem. Phys. Lett.* **144**, 1–5 (1988).
[26] Gautam, K. S., Kumar, S., Wermeille, D., Robinson, D., and Dhinojwala, A., *Phys. Rev. Lett.* **90**, 215501/1–4 (2003).
[27] Gautam, K. S., Molecular Structure and Order-to-Disorder Transitions of Comb Polymer at Air and Solid Interfaces Ph.D. Thesis, The University of Akron, Akron, OH, 2002.
[28] Gautam, K. S. and Dhinojwala, A., *Phys. Rev. Lett.* **88**, 145501/1–4 (2002).
[29] Tsige, M., Soddemann, T., Rempe, S. B., Grest, G. S., Kress, J. D., Robbins, M. O., Sides, S. W., Stevens, M. J., and Webb, E., III, *J. Chem. Phys.* **118**, 5132–5142 (2003).
[30] Harp, G., Rangwalla, H., Yeganeh, M. S., and Dhinojwala, A., *J. Am. Chem. Soc.* **125**, 11283–11290 (2003).
[31] Schwab, A. D. and Dhinojwala, A., *Phys. Rev. E* **67**, 021802/1–10 (2003).